AIAA 81-4076

Equilibrium Spinning of a Typical Single-Engine Low-Wing Light Aircraft

Barnes W. McCormick*
The Pennsylvania State University, University Park, Pa.

A study is performed of rotary balance data, spin tunnel model, radio-controlled (R/C) model, and full-scale flight test results relating to the spinning of light aircraft. A method is presented for predicting steady spin modes using rotary balance data. Differences in spin characteristics of various wing, tail, and fuselage modifications are discussed as well as scale effects. It is concluded that an equilibrium flat spin is governed primarily by the yawing moment coefficient.

Nomenclature

C_Ω = moment coefficient about spin axis, Eq. (12)
N_s = yawing moment about spin axis
R_s = spin radius
θ = pitch angle of aircraft x axis measured from vertical; θ = angle of attack for vertical descent with zero value of R_s
σ = helix angle for c.g. path
$\bar{\omega}$ = dimensionless spin rate, $\Omega b/2V$
Ω = spin rate, rad/s

Subscripts

i = inertia
net = sum of aerodynamic and inertial coefficients

Introduction

A "TYPICAL single-engine low-wing general aviation design," has been intensively investigated with regard to its spin characteristics by NASA Langley. Wind tunnel testing has included static tests at model and full-scale Reynolds numbers[1] and rotary balance testing at model Reynolds numbers.[2-5] Free-flight spin testing has been performed using spin-tunnel models (1/11 scale), radio-controlled (R/C) models (1/5 scale) and a full-scale airplane.[6-9] Model and full-scale Reynolds numbers, based on the MAC, for the static tests were approximately 0.3×10^6 and 3.5×10^6, respectively. R_e for the rotary balance data and for the spin-tunnel models was approximately the same and equal to 0.13×10^6. A three-view drawing of the basic full-scale airplane is presented in Fig. 1; while Fig. 2 presents some of the modifications that were tested. The principal modifications include varying the vertical position of the horizontal tail and adding full-span or partial-span droop to the wing's leading edge. The other modifications are to the fuselage.

The purpose of this study is to analyze the spin characteristics of the model and full-scale airplane using rotary balance data. A graphical method is developed for predicting fully-developed spin modes from the rotary balance. Reasons are offered for differences in the spin performance of the various tail and fuselage modifications.

Analysis: Reduction of the Equations of Motion

The equations of motion of a rigid airplane having six degrees of freedom, assuming all products of inertia to equal approximately zero, reduce to the following for steady motion:[15]

$$L=(I_z-I_y)QR \tag{1a}$$

$$M=-(I_z-I_x)RP \tag{1b}$$

$$N=(I_y-I_x)PQ \tag{1c}$$

$$X=m(Qw-Rv) \tag{1d}$$

$$Y=m(-Pw+Ru) \tag{1e}$$

$$Z=m(Pv-Qu) \tag{1f}$$

The path of the c.g. of a spinning airplane prescribes a helix as the airplane descends. The axis of the helix is vertical and the radius of the helix is referred to as the spin radius. This parameter and pertinent angles are shown in Fig. 3.

If the spin radius is taken to be approximately equal to zero then the rotation rates P,Q, and R about the airplane axes are related to the rotation rate about the spin axis Ω and the roll angle ϕ by

$$P=\Omega\cos\theta \tag{2a}$$

$$Q=\Omega\sin\theta\sin\phi \tag{2b}$$

$$R=\Omega\sin\theta\cos\phi \tag{2c}$$

If one examines the resultant velocities along the span of a spinning wing, the accuracy of assuming the spin radius R_s to equal zero will be seen to depend on the ratio of R_s to the wing

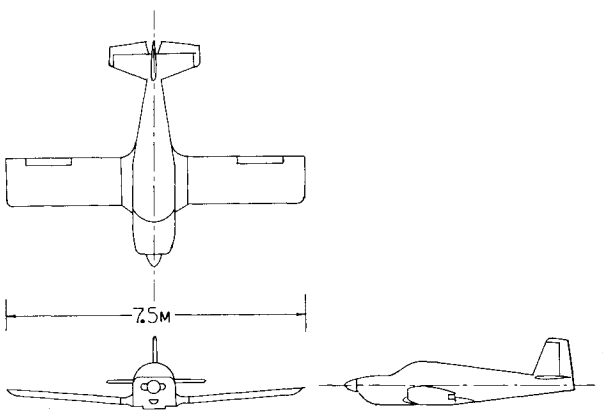

Fig. 1 Typical single-engine, low-wing general aviation airplane.

Received March 20, 1980; revision received Aug. 21, 1980. This paper is declared a work of the U.S. Government and therefore is in the public domain.

*Professor and Head, Department of Aerospace Engineering. Associate Fellow AIAA.

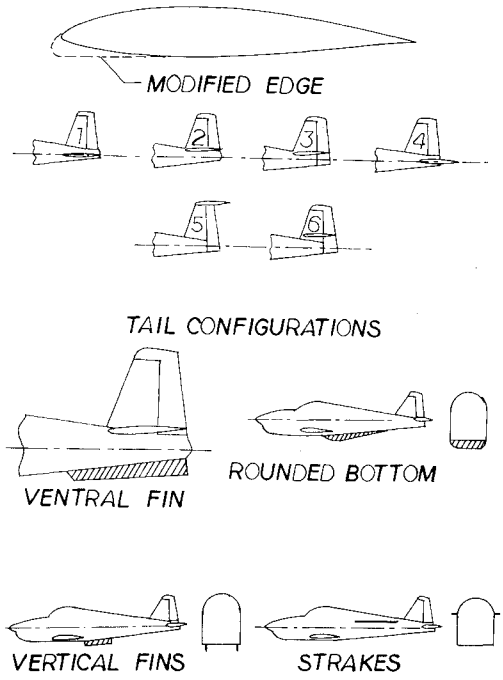

Fig. 2 Modifications tested.

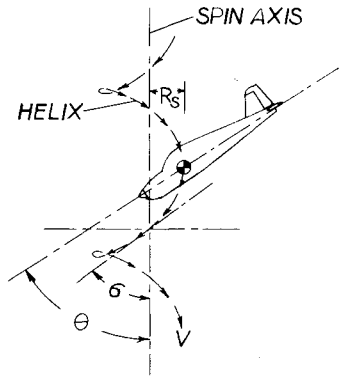

Fig. 3 Path and attitude of a spinning airplane.

span, b. R_s can be calculated approximately by assuming the resultant aerodynamic force on the airplane to be normal to the airplane's x-y axes. Physically, the airplane is nosed in toward the spin axis so that the normal force, inclined inward, balances the centrifugal force so that,

$$R_s = g/(\Omega^2 \tan\theta) \tag{3}$$

Equation (3) dates, at least, to 1936 where it can be found in Ref. 10.

The velocity components along the airplane axes can be written in terms of the vertical velocity of descent V and the pitch and roll angles θ and ϕ. Note that θ is measured from the vertical.

$$u = V\cos\theta \tag{4a}$$

$$v = V\sin\theta\sin\phi \tag{4b}$$

$$w = V\sin\theta\cos\phi \tag{4c}$$

The helix angle σ and the sideslip angle β then becomes,

$$\sigma = \sin^{-1}(\Omega R_s/V) \tag{5}$$

$$\beta = \phi - \sigma \tag{6}$$

Table 1 Typical spin characteristics with tail 4

	Spin-tunnel model	R/C model	Full-scale airplane
		Flat spin	
θ deg	77	~80 est.	53
ϕ deg	1	...	0
$\bar{\omega}$	0.91	4.8 rad/s[a]	0.45
R_s/b	0.20	...	0.06
σ deg	21.3	...	3.1
β deg	−20.3	...	−3.1
		Steep spin	
θ deg	35	~45	40
ϕ deg	−2.5	...	8
$\bar{\omega}$	0.24	3.1 rad/s[a]	0.27
R_s/b	0.23	...	0.20
σ deg	6.3	...	6.0
β deg	−8.8	...	2.0

[a] Descent rate not measured; Ω tabulated.

If the set of Eqs. (4) are substituted into the set of Eqs. (1) and nondimensionalized, the following equations result:

$$C_x = C_y = C_z = 0 \tag{7a}$$

$$C_l = \bar{\omega}^2 (i_z - i_y)\sin^2\theta\sin\phi\cos\phi \tag{7b}$$

$$C_m = -\bar{\omega}^2 (b/\bar{c})(i_z - i_x)\cos\theta\sin\theta\cos\phi \tag{7c}$$

$$C_n = \bar{\omega}^2 (I_y - i_x)\cos\theta\sin\theta\sin\phi \tag{7d}$$

where,

$$C_l = l/qSb \qquad C_x = X/qS \qquad i_x = I_x/\rho Sb^3$$
$$C_m = M/qS\bar{c} \qquad C_y = Y/qS \qquad i_y = I_y/\rho Sb^3$$
$$C_n = N/qSb \qquad C_z = Z/qS \qquad i_z = I_z/\rho Sb^3$$

Normally, for light, single-engine aircraft, $i_z > i_y > i_x$.

At this point, it would appear that there are six equations for the six coefficients and only three unknowns: $\bar{\omega}$, θ, and ϕ. However, consider the force along the vertical spin axis. This resultant force from Eq. (7a) must equal zero. Hence,

$$W + X\cos\theta + Z\sin\theta\cos\phi + Y\sin\phi\sin\theta = 0$$

or,

$$W = -qS(C_x\cos\theta + C_y\sin\theta\sin\phi + C_z\sin\theta\cos\phi) \tag{8}$$

C_x, C_y, and C_z are aerodynamic force coefficients that depend upon $\bar{\omega}$, θ, and ϕ. If values of $\bar{\omega}$, θ, and ϕ are found to satisfy the three moment equations, then q can be adjusted to satisfy Eq. (8). Thus, the rate of descent represents another unknown. To balance the remaining forces requires a relaxation of the restriction of a zero spin radius. Also, one should allow for an angular rotation angle ψ about the airplane's z axis in addition to the angle ϕ already considered. Thus, R_s, q, and ψ represent the remaining three unknowns required to solve the set of Eq. (8).

The approach to be followed here, similar to that taken by others,[11-13] is to satisfy only the moment equations Eqs. (7b-d). These represent three equations in the unknowns $\bar{\omega}$, θ, and ϕ.

A particular combination of these three variables which provide moment equilibrium is referred to as a spin mode. Generally an airplane may exhibit one or more spin modes. In the case of two modes, these are usually designated as being steep or flat depending upon the angle θ. Varying degrees of flatness or steepness are indicated by labeling the spin as moderately flat. The boundaries between these mode shapes are not well defined. Table 1 presents some typical ex-

perimental values of $\bar{\omega}$, θ, and ϕ for the tail 4 configuration which exhibits two definite spin modes. In the case of the model one might say that one mode is a flat spin while the other one is steep. However, because of scale effects, both of these modes become more moderate for the full-scale airplane.

A configuration that exhibits only one mode may trim at any θ value between approximately 30 and 80 deg. That is to say, simply because an airplane exhibits only one mode does not mean that the single mode will necessarily be steep or flat; it may be moderate in θ. Also, it takes time for a spin to become full developed. Initially, following a stall, a light plane may drop off into what appears to be a steep spin from which recovery is possible. However, if the controls are held in the prospin positions and recovery is not effected, the spin rate can gradually increase with the nose coming up into a stable flat spin from which recovery may not be possible. Four or five complete turns can be required before an equilibrium spin condition is reached.

Application of Rotary Balance Data to the Solution of the Moment Equations

The solution to be described of Eqs. (7b-d) is graphical in nature. While the procedure can be performed with a computer, the manual execution of the process provided a valuable insight into the behavior of the aerodynamic coefficients as a function of θ, ϕ and $\bar{\omega}$. To begin, a net moment coefficient about each axis is defined as the sum of the aerodynamic coefficient and an inertial coefficient.

$$C_l = C_{l_a} + C_{l_i} \tag{9a}$$

$$C_m = C_{m_a} + C_{m_i} \tag{9b}$$

$$C_n = C_{n_a} + C_{n_i} \tag{9c}$$

where

$$C_{l_i} = -\bar{\omega}^2 (i_z - i_y) \sin^2\theta \sin\phi\cos\phi \tag{10a}$$

$$C_{m_i} = \bar{\omega}^2 (b/\bar{c}) (i_z - i_x) \cos\theta\sin\theta\cos\phi \tag{10b}$$

$$C_{n_i} = -\bar{\omega}^2 (i_y - i_x) \cos\theta\sin\theta\sin\phi \tag{10c}$$

As a word of caution, some references define C_m in terms of b instead of $\bar{c}$. The notation used here is consistent with the rotary balance data reported in Refs. 1-5 and with most treatments of longitudinal stability.

Instead of considering the trim of the yawing moment C_n it was felt that the yawing moment about the spin axis might be more instructive with regard to autorotation. Thus, a moment coefficient about the spin axis C_Ω is defined by

$$C_\Omega = (N_s/qSb) \tag{11}$$

C_Ω can be obtained by resolving the other three moments about the spin axis. Keeping in mind that C_m is defined in terms of $\bar{c}$, C_Ω becomes

$$C_\Omega = C_l\cos\theta + C_m (\bar{c}/b) \sin\phi\cos\theta + C_n\cos\phi\sin\theta \tag{12}$$

In the graphs to follow, the aerodynamic moment coefficients were taken directly from Refs. 2-5. For most of the data, it was necessary to estimate effects of control deflections. In a spin the wing is stalled nearly completely and the flow over the empennage is separated. Thus, the dependence of C_l, C_m, and C_n on control positions is generally nonlinear. This is illustrated in Fig. 4 for typical flat and steep spin conditions. The aileron deflection is positive when the right aileron is down. Note that, for the flat spin, aileron control

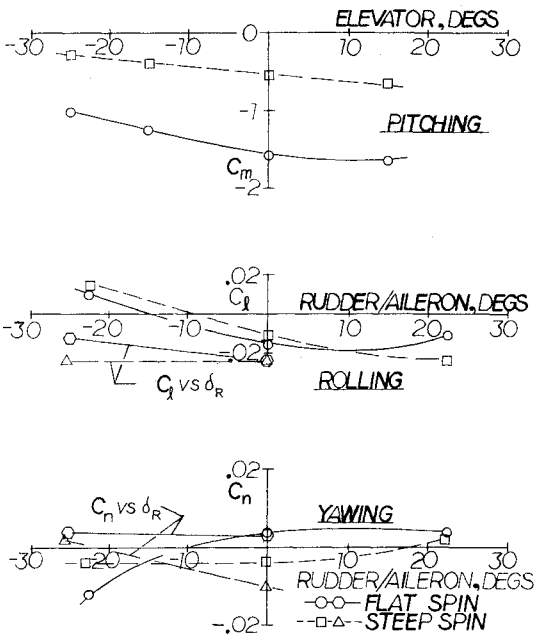

Fig. 4 Effectiveness of controls in steep and flat spins.

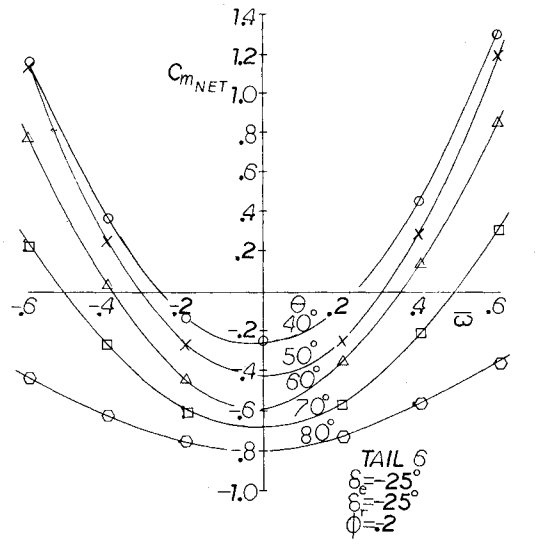

Fig. 5 Typical pitching moment as a function of spin rate and pitch attitude.

against the spin produces a prospin yawing moment while the rudder has little or no effect. For the steep spin, the rudder is effective while ailerons against spin show a slight antispin yawing moment.

The basic procedure is relatively simple in concept. For a given airplane configuration (geometry, inertias, and control positions), the following steps are performed.

1) Plot C_m (net) vs $\bar{\omega}$ for constant values of ϕ and θ.

2) From cross plots of $C_m = 0$, graph θ vs $\bar{\omega}$ for constant ϕ values to trim C_m.

3) Plot C_l (net) vs ϕ for constant values of θ and $\bar{\omega}$.

4) Cross plot θ vs $\bar{\omega}$ for constant values of ϕ to trim C_l to zero.

5) Superimpose the results from steps 2 and 4 to obtain either θ or $\bar{\omega}$ as a function of ϕ to trim C_m and C_l simultaneously.

6) Plot C_Ω (net) vs $\bar{\omega}$ for constant values of ϕ and θ.

7) Cross plot θ vs $\bar{\omega}$ for constant values of ϕ to trim C_Ω to zero.

8) Superimpose the results from steps 2 and 7 to obtain either θ or $\bar{\omega}$ as a function of ϕ to trim C_m and C_Ω simultaneously.

9) Superimpose the results from steps 5 and 8 to obtain a combination, or combinations of θ, $\bar{\omega}$, and ϕ that will trim simultaneously C_m, C_l, and C_Ω to zero. Such a combination represents a predicted equilibrium spin mode.

These steps were derived from a trial and error process that disclosed problems with other approaches. For example, it was found that C_l as a function of $\bar{\omega}$ for constant values of θ and ϕ is highly nonlinear making interpolation very difficult. When plotted against ϕ however, C_l is well behaved. This is not to imply that accomplishment of the listed steps is not without its problems. Generally these relate to the nonlinear nature of the data. To accurately define trim points will require rotary balance data at more closely spaced ϕ values than reported in Refs. 2-5.

Typical curves for tail 6 of C_m, C_l, and C_Ω are presented in Figs. 5-7. Obviously, cross plots for C_Ω equal to zero are done with some amount of trepidation. Further, in predicting equilibrium modes, static stability should be considered. Thus, only trim points are plotted for which the following conditions hold:

$$\frac{\partial C_m}{\partial \theta} < 0 \qquad \phi, \bar{\omega} \text{ const}$$

$$\frac{\partial C_l}{\partial \phi} < 0 \qquad \theta, \bar{\omega} \text{ const}$$

$$\frac{\partial C_l}{\partial \bar{\omega}} < 0 \qquad \theta, \phi \text{ const}$$

Static stability in pitch is emphasized further by Fig. 8. Here C_m is plotted against θ for constant values of $\bar{\omega}$. The net pitching moments, for the stalled conditions of a spin, do not depend greatly on ϕ or on the vertical position of the horizontal tail; hence, these curves hold approximately for all ϕ values of interest and tail configurations. The slopes of these curves become increasingly more negative for zero C_m as θ increases; i.e., as the spin becomes more flat. Thus, in pitch, the airplane tends to "lock in" as the spin flattens out.

A prediction of θ as a function of $\bar{\omega}$ to trim C_m based on rotary balance data is presented in Fig. 9. Test points from spin tunnel and full-scale testing are included on the figure where the correlation between the predicted and experimental data is seen to be good. This suggests that θ vs $\bar{\omega}$ to trim C_m is not dependent upon Reynolds number. It also indicates that the trim C_m is not too dependent upon horizontal tail placement since the data points represent several tail configurations including ventral fin additions.

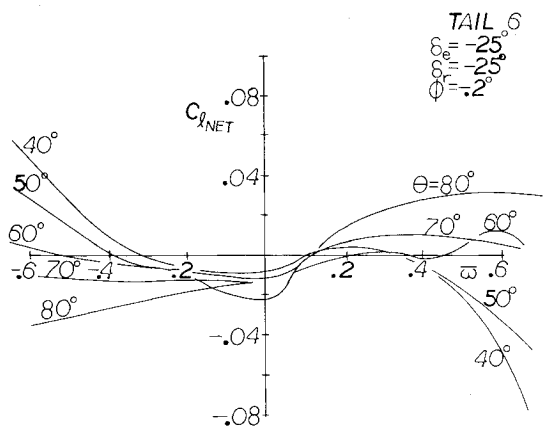

Fig. 6 Typical rolling moment coefficient as a function of spin rate and pitch attitude.

Final predictions, based on rotary balance data, of equilibrium spin modes are presented in Figs. 10 and 11 for tails 6 and 3. Experimental equilibrium points obtained with models in Langley's spin tunnel are also shown. Qualitatively, the predictions compare favorably with the experimental observations. Tail 6 was observed to have only one spin mode in agreement with only one intersection of the two curves along which the moments are trimmed. Tail 3 is predicted to have both a steep and flat spin mode which is also in agreement with spin tunnel tests.

Quantitatively, the predictions are close to the experimental results for tail 6 but are not so close for tail 3. Nevertheless, the agreement between the rotary balance data and spin tunnel observations is gratifying in view of the difficulties encountered in interpolating the rotary balance data, particularly the yawing moment coefficient C_n.

Examination of Factors Affecting Spin Characteristics

We will now examine what appears to be the basic reason for tail 3 having a flat spin mode as compared to only a steep mode for tail 6. Figure 12 presents a comparison of the net

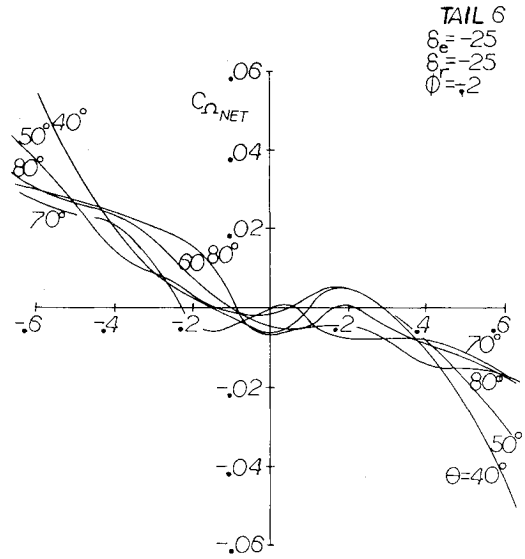

Fig. 7 Typical moment coefficient about the spin axis as a function of spin rate and pitch attitude.

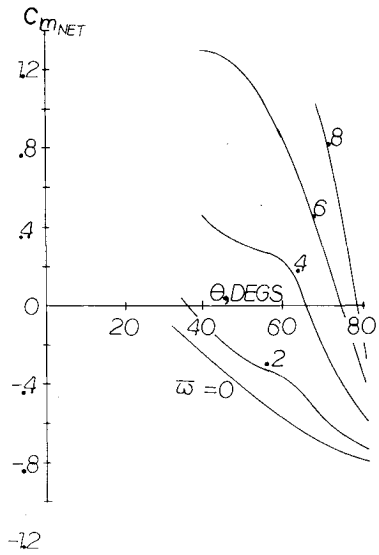

Fig. 8 Pitching moment as a function of pitch attitude for constant spin rates.

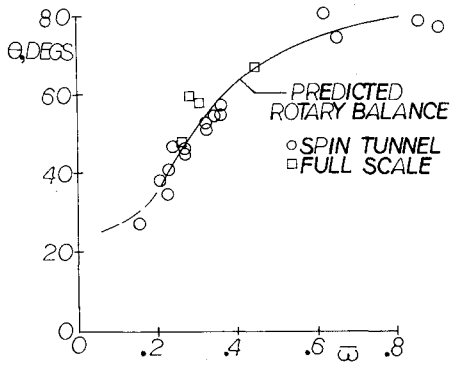

Fig. 9 Pitch attitude to trim pitching moment as a function of spin rate.

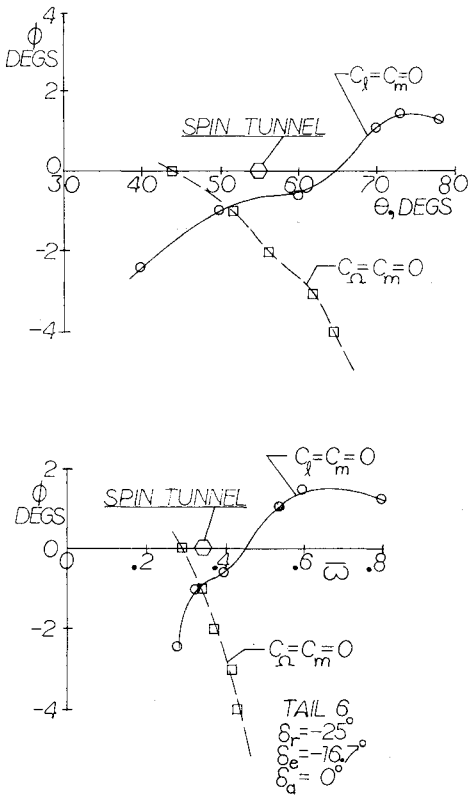

Fig. 10 Predicted spin equilibrium for configuration having one spin mode.

moment coefficients for the two tails around conditions corresponding to the flat spin mode. Figure 13 is the same kind of comparison for the steep spin mode. From a study of these figures, it is concluded that the major difference between the two tails lies with the autorotational moment coefficient, C_Ω. The curves are otherwise similar but C_Ω, for tail 6, will not trim to zero for any θ at this low roll angle and relatively high spin rate.

It is interesting at this point to note that tail 2 does not spin flat. The geometry of this tail is identical to tail 3 except that the rudder for tail 2 does not extend below the horizontal tail. Apparently, the more effective rudder on tail 3 provides a sufficiently positive increment in C_n at high θ and $\bar{\omega}$ values to trim the autorotational moment whereas the rudder of tail 2 does not. In this regard, the more effective rudder is less desirable. Of course, this may not be true in considering spin entry. The most stringent requirement for equilibrium in a flat spin appears to be C_Ω. At high θ and low ϕ values, C_Ω and C_n are nearly equal, and the inertia moment about the spin axis is small. Thus, for the possibility of a flat spin, or for assessing

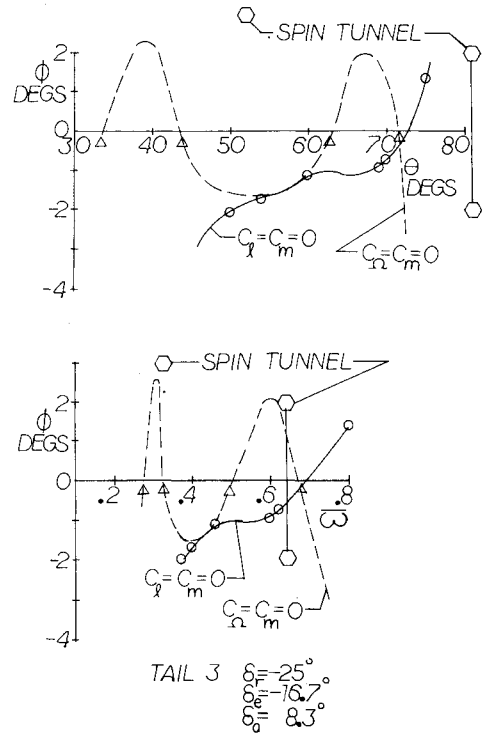

Fig. 11 Predicted spin equilibrium for configuration having two spin modes.

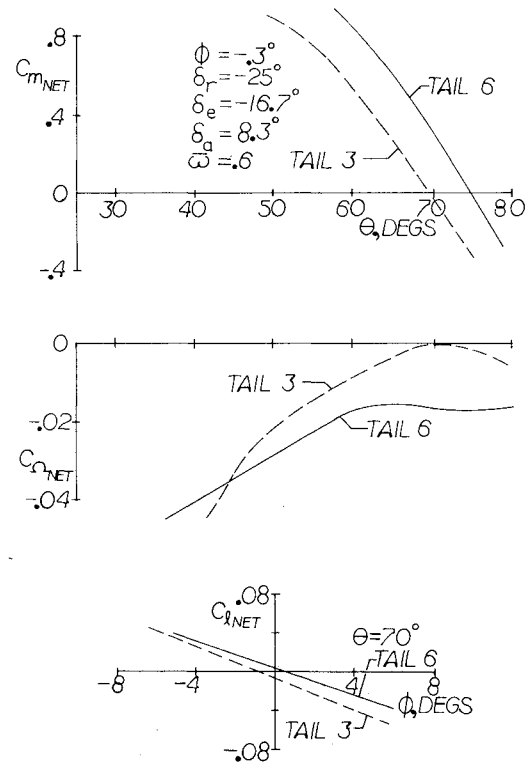

Fig. 12 Comparison of moment coefficients between tails 3 and 6 for the flat spin mode.

one configuration against another, it is instructive to examine the aerodynamic yawing moment C_n as a function of θ at a value of $\bar{\omega}$ that is typical of a flat spin. Figures 14 and 15 provide such a comparison for most of the tails and modifications reported in the references at the model Reynolds number and zero control deflections. Typically, these C_n values can be increased by 0.005 to 0.010 by

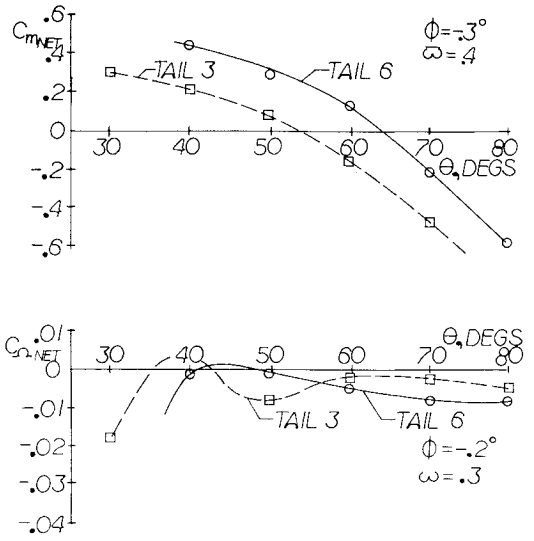

Fig. 13 Comparison of moment coefficients between tails 3 and 6 for the steep spin mode.

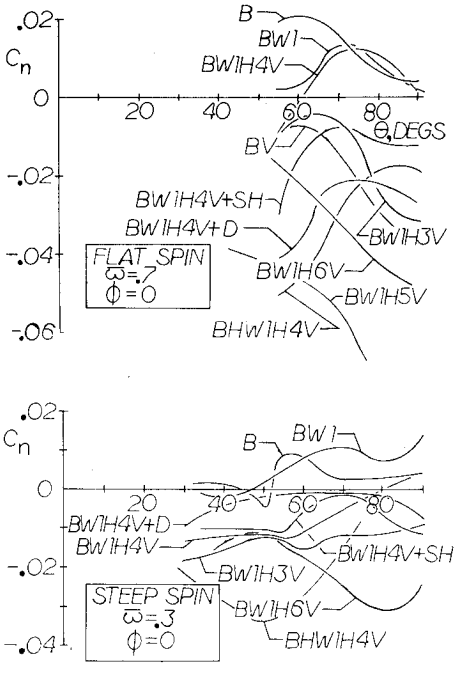

Fig. 14 Effect of configuration on the yawing moment coefficient for flat and steep spin conditions.

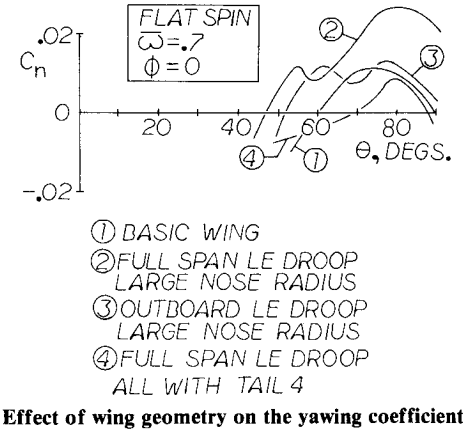

Fig. 15 Effect of wing geometry on the yawing coefficient for a flat spin.

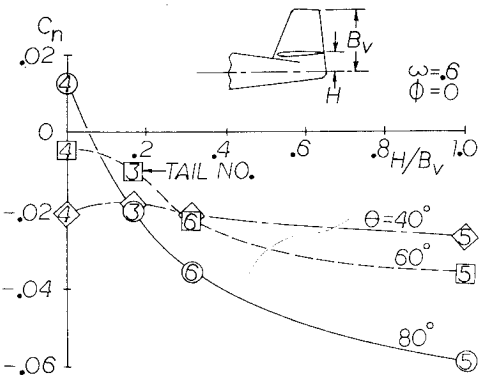

Fig. 16 Effect of horizontal tail position on yawing moment for flat spin.

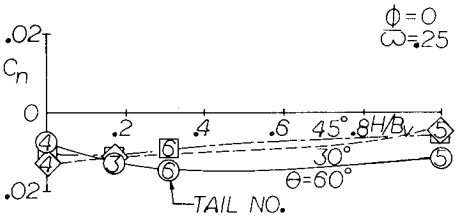

Fig. 17 Effect of horizontal tail position on yawing moment for the steep spin.

deflecting the rudder to −25 deg. On Fig. 14 B denotes body; W1 the basic wing; H4 the horizontal tail (tail 4 in this case); V the vertical tail; while +D and +SH denote a deep-rounded bottom and side-horizontal strakes, respectively, added to the fuselage. The data presented in Fig. 15 were all taken with tail 4.

The configurations which exhibited flat spins in the spin tunnel were BW1H3V and BW1H4V. The horizontal strakes (BW1H4V + SH) were only slightly effective while the deep-rounded bottom (BW1H4V+D) eliminated the flat spin. Tails 5 and 6 did not spin flat nor did tail 4 with a high wing. The spin tunnel results to date are consistent with Figs. 14 and 15. Those configurations with C_n values less than approximately −0.01 over θ values from 55 to 90 deg did not spin flat.

The basic wing, in a flat spin at a high $\bar{\omega}$, contributes little to autorotation.[14] Below θ values of 70 deg, the wing is providing a damping moment. The autorotational moment with the basic wing is provided by the fuselage. This conclusion is based on a comparison of the fuselage along (B) with the wing plus fuselage curve (BW1). For steeper spins at lower $\bar{\omega}$ values, the wing and fuselage both contribute to the autorotational moment although at a θ value below approximately 50 deg, the contribution from the fuselage diminishes rapidly.[16] Drooping the leading edge and increasing the nose radius increases significantly the wing's autorotational moment in a flat spin.

The yawing moment coefficient C_n is presented in Fig. 16 as a function of the vertical placement of the horizontal tail for constant values of θ and an $\bar{\omega}$ of 0.6 representative of flat spin conditions. Figure 17 typifies a steep spin with $\bar{\omega}$ equal to 0.25. Notice that raising the horizontal tail has little or no effect on yaw damping for the steep spin. However, for the flat spin, yaw damping is increased by raising the horizontal tail for θ values above 40 deg.

Inertia Moments

It is instructive to examine the variation of the inertia moments with θ and ϕ. Combining Eqs. (7), (10), and (12), the

inertial moment about the spin axis becomes

$$C_{\Omega_i} = -\bar{\omega}^2 (I_z - i_y) \sin^2\theta\cos\theta\sin\phi\cos\phi + \bar{\omega}^2 (I_z - i_x) \cos^2\theta\sin\theta\sin\phi\cos\phi - \bar{\omega}^2 (i_y - i_x) \cos\theta\sin^2\theta\sin\phi\cos\phi \quad (13)$$

If ϕ is assumed to be a small angle, then $C_{\Omega i}$ reduces to

$$C_{\Omega_i} = \bar{\omega}^2 \phi\sin\theta\cos\theta(\cos\theta - \sin\theta)\,(i_z - i_x) \quad (14)$$

Normally, for a light aircraft, $I_z > I_y > I_x$ so that the inertial rolling moment is stabilizing for all θ values. $dC_{m_i}/d\theta$ is destabilizing up to a θ of 45 deg but changes sign at the higher θ values. The inertial yawing moment about the spin axis is autorotative below θ values of 45 deg for positive ϕ's. Above 45 deg, C_{Ω_i} becomes negative.

Notice that because of the assumption that ϕ is small, the inertia moment about the spin axis is proportional to $(I_z - I_x)$. However, the quantity $(I_x - I_y)$ is often seen as a principal parameter against which spin performance is measured. Specifically, an inertia yawing-moment parameter (IYMP) is defined as,

$$\text{IYMP} = (I_x - I_y)/(mb^2) \quad (15$$

This factor is important with regard to spin entry where ϕ is large. However, from Eq. (14) the quantity $(i_z - i_x)$ appears to be a more meaningful dimensionless pararameter against which to correlate equilibrium spin performance. It is of interest to note that moving the c.g. from 0.145 $\bar{c}$ to 0.255$\bar{c}$ has little effect on the equilibrium spin models tested in the spin tunnel. Similarly, moving the c.g. from 0.26 $\bar{c}$ to 0.35$\bar{c}$ does not affect the moderately flat equilibrium spin for the full-scale configuration, tail 4.

Full-Scale Flight Test Data

The full-scale flight tests are being conducted at the NASA facility at Wallops Island, Va. The airplane is completely instrumented to provide time histories of all parameters pertinent to the spin problem. The spin is initiated at an altitude of approximately 2800 m (9000 ft). At approximately 1500 m (5000 ft), if the airplane has not recovered from the spin, a spin chute attached to the tail is opened to arrest the spin. This chute has been used several times to date in order to recover from flat spins.

It has been observed that many configurations do not exhibit a steep spin mode. Rather, upon initiation of the spin, holding full rudder and up elevator, the airplane continuously increases its spin rate and flattens the spin. The tendency to go flat is recognizable by the test pilot so that a recovery can be made by the application of opposite rudder and down elevator before the spin becomes so flat that the spin chute is needed. Ailerous against the spin are of no help in the recovery. In fact, opposite ailerons tend to flatten the spin and increase the spin rate.

Observations on the Model and Full-Scale Flight Tests

Based on the results presented in Refs. 6-9, the following observations are made.

1) Tails 1, 3, and 4 exhibited flat, unrecoverable spin modes in the spin tunnel.

2) Tail 3 did not spin flat for either the R/C model or the full-scale airplane.

3) Tail 4 spun flat for the full-scale airplane and R/C model but required a particular sequencing of the elevator to do so.

4) Adding the rounded bottom, ventral fin, and vertical fins to tail 4 were effective in eliminating the flat spin in the spin tunnel. The side, horizontal strakes for tail 4 were partially successful.

5) Full-span, leading edge droop did not change the characteristics of the spin tunnel models.

6) Tails 2-4 and 6 spun flat on the full-scale airplane with full-span, leading-edge droop although tail 6 was recoverable.

7) On the R/C model, tail 4 readily spun flat with full-span droop without special elevator sequencing.

8) Outboard leading-edge droop, with a discontinuity at the juncture of the droop and the basic wing, eliminated the flat spin for both the R/C model and the full-scale airplane with tail 4.

9) Fairing the discontinuity at the juncture of the outboard, leading-edge droop, and basic wing eliminated the beneficial effects on the full-scale airplane previously noted for the outboard droop.

10) The full-scale airplane with full-span droop spun flat with the addition of the rounded bottom fuselage, with the horizontal strakes, with the vertical fins, and with the ventral fin.

Conclusions

Based on the graphical analysis of the rotary balance data and observations of model and full-scale tests, a number of conclusions are reached for this type of configuration.

1) Depending upon the configuration, there may be significant differences in the spin characteristics due to Reynolds number for the spin tunnel models when compared with either the R/C models or the full-scale airplane. The R/C model and full-scale airplane give consistent results.

2) The basic wing provides little or no prospin yawing moment in a flat spin. The moment is provided by the fuselage.

3) Leading-edge droop, maintaining the same nose radius, provides and appreciable prospin yawing moment in a flat spin at higher Reynolds numbers but not at low values of R_e. However, increasing the nose radius with droop also increases the prospin yawing moment at model R_e values.

4) Rotary balance data is reliable and can be used to predict equilibrium spin modes. However, for full-scale predictions, Reynolds number effects may be important.

5) For purposes of analysis, rotary balance data should be taken at ϕ values of 0,2,4 and 6 deg. Angles in excess of 6 deg are not needed, at least for light aircraft. The four values of ϕ are needed mainly to interpolate accurately the yawing moment as a function of ϕ, θ, and $\bar{\omega}$.

6) Tail 4, for the full-scale airplane, exhibited two distinct spin modes, but it requires some manipulation of the controls to get into the flat mode. Configurations which spin flat readily transist continuously into the flat mode and thus may not have a stable, steep mode.

7) Rotary balance data shows no significant difference between full-span and outboard leading-edge droop at flat spin conditions.

8) For the flat spin, and probably for the steep spin, a zero spin radius is a good assumption for studying spin mode characteristics.

9) In a flat spin, raising the horizontal tail increases yaw damping; however, in a steep spin the tail position has little effect on C_n.

Acknowledgment

This study was performed at the NASA Langley Research Center while on sabbatical leave. The assistance of personnel of the Dynamic Stability Branch is gratefully acknowledged.

References

[1] Bihrle, W., Barnhart, B., and Pantason, P., "Static Aerodynamic Characteristics of a Typical Single-Engine Low-Wing

General Aviation Design for an Angle-of-Attack Range of −8° to 90°," NASA CR-2971, July 1978.

[2]Bihrle, W., Hultberg, R.A., and Mulcay, W., "Rotary Balance Data for a Typical Single-Engine Low-Wing General Aviation Design for an Angle-of-Attack Range of 30° to 90°," NASA CR-2972, July 1978.

[3]Hultberg, R.S. and Mulcay, W., "Rotary Balance Data for a Typical Single-Engine General Aviation Design for an Angle-of-Attack Range of 8° to 90°. I-Low-Wing Model A," NASA CR-3100, Feb. 1979.

[4]Mulcay, W. and Rose, R., "Rotary Balance Data for a Typical Single-Engine, General Aviation Design for an Angle-of-Attack Range of 8° to 90°. II-High-Wing Model A," NASA CR-3101, Feb. 1979.

[5]Bihrle, W. and Mulcay, W., "Rotary Balance Data for a Typical Single-Engine Design for an Angle-of-Attack Range of 8° to 35°. III-Effect of Wing Leading-Edge Modifications Model A," NASA CR-3102, Feb. 1972.

[6]Burk, A.M., Bowman, J.A., and White, W.L., "Spin-Tunnel Investigation of the Spinning Characteristics of Typical Single-Engine General Aviation Airplane Designs," NASA TP-1009, Sept. 1977.

[7]Bowman, J.A., Burk, S.M., Stough, H.P., and Patton, J.M., "Correlation of Model and Airplane Spin Characteristics for a Low-Wing General Aviation Research Airplane," AIAA Paper 78-1477, Aircraft Systems and Technology Conference, Los Angeles, Calif., Aug. 1978.

[8]DiCarlo, D.J. and Johnson, J.L., "Exploratory Study of the Influence of Wing Leading-Edge Modifications on the Spin Characteristics of a Low-Wing, Single-Engine General Aviation Airplane," AIAA Paper 79-1837, Aircraft Systems and Technology Meeting, New York, N.Y., Aug. 1979.

[9]Stough, H.P. and Patton, J.M., "The Effects of Configuration Changes on Spin and Recovery Characteristics of a Low-Wing General Aviation Research Airplane," AIAA Paper 79-1786, Aircraft Systems and Technology, New York, N.Y., Aug. 1979.

[10]Zimmerman, C.H., "Preliminary Tests in the NACA Force-Spinning Wind Tunnel," NACA 557, 1936.

[11]Graham, A.B., "Prediction of the Flat Spin Characteristics of a Fighter Airplane," M.S. Thesis, George Washington Univ., April 1976.

[12]Williams, D.A., "The Use of Rotation-Balance Data in Theoretical Spin Studies," M.S. Thesis, George Washington Univ., Aug. 1976.

[13]Tischler, M.B. and Barlow, J.B., "Application of the Equilibrium Spin Technique to a Typical Low-Wing General Aviation Design, AIAA Paper 79-1625, Atmospheric Flight Mechanics Conference, Boulder, Colo., Aug. 6-8, 1979.

[14]Bamber, M.J. and Zimmerman, C.H., "Spinning Characteristics of Wings I Rectangular Clark-Y Monoplane Wing," NACA 519, 1935.

[15]McCormick, B.W., *Aerodynamics, Aeronautics and Flight Mechanics,* John Wiley and Sons, New York, N.Y., 1979.

[16]Clarkson, M.H., "Autorotation of Fuselages," IAS Preprint 770, presented at 26th Annual Meeting of Institute of Aeronautical Sciences, Jan. 1958.